CrossMark

ARTICLE

In-Situ Hydrothermal Synthesis of Bi–Bi$_2$O$_2$CO$_3$ Heterojunction Photocatalyst with Enhanced Visible Light Photocatalytic Activity

Prasenjit Kar[1] · Tuhin Kumar Maji[1] · Ramesh Nandi[1] ·
Peter Lemmens[2,3] · Samir Kumar Pal[1]

Highlights

- A facile low cost hydrothermal technique was employed to synthesize of Bi-Bi$_2$O$_2$CO$_3$, and Bi nanoparticles was decorated in-situ on Bi$_2$O$_2$CO$_3$.
- The heterostructure exhibits enhanced electron-hole separation and improves visible-light photocatalytic activity effectively.

Abstract Bismuth containing nanomaterials recently received increasing attention with respect to environmental applications because of their low cost, high stability and nontoxicity. In this work, Bi–Bi$_2$O$_2$CO$_3$ heterojunctions were fabricated by in-situ decoration of Bi nanoparticles on Bi$_2$O$_2$CO$_3$ nanosheets *via* a simple hydrothermal synthesis approach. X-ray diffraction (XRD), scanning electron microscopy (SEM), transmission electron microscopy (TEM) and high-resolution TEM (HRTEM) were used to confirm the morphology of the nanosheet-like heterostructure of the Bi–Bi$_2$O$_2$CO$_3$ composite. Detailed ultrafast electronic spectroscopy reveals that the in-situ decoration of Bi nanoparticles on Bi$_2$O$_2$CO$_3$ nanosheets exhibit a dramatically enhanced electron-hole pair separation rate, which results in an extraordinarily high photocatalytic activity for the degradation of a model organic dye, methylene blue (MB) under visible light illumination. Cycling experiments revealed a good photochemical stability of the Bi–Bi$_2$O$_2$CO$_3$ heterojunction under repeated irradiation. Photocurrent measurements further indicated that the heterojunction incredibly enhanced the charge generation and suppressed the charge recombination of photogenerated electron-hole pairs.
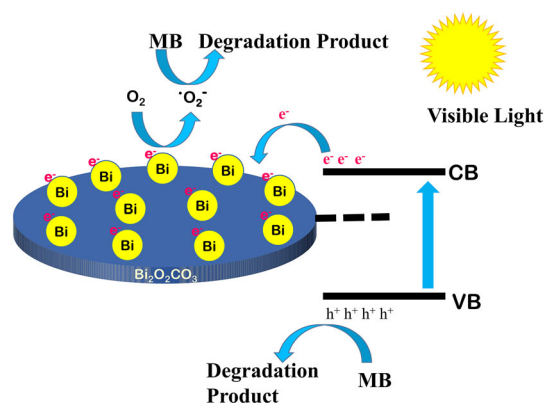
✉ Samir Kumar Pal
  skpal@bose.res.in

1 Department of Chemical Biological and Macromolecular Sciences, S. N. Bose National Centre for Basic Sciences, Block JD, Sector III, SaltLake, Kolkata 700106, India

2 Institute for Condensed Matter Physics, TU Braunschweig, Mendelssohnstraße 3, 38106 Brunswick, Germany

3 Laboratory for Emerging Nanometrology, TU Braunschweig, Brunswick, Germany

1 Introduction

Photocatalysis technology has attracted enormous interest because of its potential to soften and release the global energy crisis and environmental pollution [1–6]. Although various types of semiconductor photocatalyst have been developed, their applications are impeded by a high recombination rate of electron–hole pairs and low efficiency of solar light absorption in the photocatalysis [7, 8]. A tremendous effort has been made to optimize the electronic band structure allowing an efficient electron–hole separation, which has been acknowledged to be a key factor in enhancing solar energy conversion [9–14]. The development of heterojunction systems has also been understood since it is beneficial for electron transfer to improve electron–hole pair separation, and therefore resulting in an excellent photocatalytic activity under solar light illumination [15, 16].

Recently, economic and abundant bismuth-containing semiconductors have been attracted large attention for diverse applications, especially in the area of energy conversion and environmental treatment [17, 18, 19, 20, 21]. The bismuth subcarbonate ($Bi_2O_2CO_3$) is one of the most interesting semiconductor with a large bang gap of 3.3 eV. It belongs to the layered Aurivillius-related oxide family, consisting of $Bi_2O_2^{2+}$ layers sandwiched between two slabs of CO_3^{2-} layers [22]. However, the use of $Bi_2O_2CO_3$ in light harvesting applications is very limited because it can absorb only UV light. To overcome this drawback, several 3D hierarchical $Bi_2O_2CO_3$ architectures composed of nanosheets, nanoplates and microspheres have been developed [23, 24]. The coupling of $Bi_2O_2CO_3$ with other materials to construct heterojunctions has also been shown as an advantages approach to improve the visible light responsive activity and to facilitate the separation of photogenerated electron–hole pairs. Different low band gap semiconductors and polymers have been used to improve the photocatalytic activity of $Bi_2O_2CO_3$. Liu et al. constructed hierarchical graphene–$Bi_2O_2CO_3$ composites which exhibit a significantly enhanced visible light photocatalytic performance [25]. Good visible light photocatalytic activity toward the degradation of Rhodamine B was reported by Zhang et al. for n–n heterostructured $Bi_2O_2CO_3$/Bi_2WO_6 [26]. Zhou's group reported that PANI decorated $Bi_2O_2CO_3$ nanosheets exhibited a four to half times better photocatalytic activity for degradation of Rhodamine B in comparison to $Bi_2O_2CO_3$ nanosheets under visible light illumination [27]. Recently, p–n heterojunction Ag_2O/$Bi_2O_2CO_3$ photocatalysts was shown to manifest an excellent visible light activity for degradation of MB and methyl orange [28].

Recently surface plasmon resonance (SPR) of noble metal nanoparticles (Ag or Au) was reported for improving the activity of semiconductor photocatalysts efficiently [29, 30]. In comparison with the high cost of noble-metals, Bi nanoparticles are inexpensive and show comparable SPR [31]. Recently, two reports on Bi nanoparticles demonstrate that they are useful for catalysis and sensing applications [32, 33]. Dong et al. showed that plasmonic Bi nanoparticles can be used for NO removal [34]. Several Bi nanoparticles based nanocomposites like Bi/BiOCl, Bi/Bi_2O_3, and Bi/BiOI exhibit enhanced photocatalytic activity comparing to their counterpart [35–37]. Recently, Bi nanoparticles based heterojunctions with semiconductor have been an intense research area due to their enhanced charge separation and improved photocatalytic efficacies [38–40]. However, Bi nanoparticles decorated $Bi_2O_2CO_3$ nanosheets have not been considered up to date.

In the present study, we developed an in situ decoration of Bi nanoparticles on $Bi_2O_2CO_3$ nanosheets via a one-pot hydrothermal method. From time-resolved fluorescence spectroscopy, we observed that an ultrafast electron transfer process in the Bi–$Bi_2O_2CO_3$ heterojunction reveals an excited state electron transfer from $Bi_2O_2CO_3$ to Bi. The novel Bi-decorated $Bi_2O_2CO_3$ nanosheets exhibited a dramatically enhanced photocatalytic activity towards MB degradation comparing to pure $Bi_2O_2CO_3$ nanosheets because of the SPR effect of Bi nanoparticles and an efficient separation of electron–hole pairs in the Bi–$Bi_2O_2CO_3$ heterojunction. We also observed that Bi–$Bi_2O_2CO_3$ exhibited a good recyclability with respect to degradation of MB, which is significant for real world applications.

2 Experimental Section

2.1 Reagents

Bismuth nitrate pentahydrate [$Bi(NO_3)_3 \cdot 5H_2O$], cityl trimethyl ammonium bromide (CTAB), sodium carbonate (Na_2CO_3), and methylene blue (MB) were purchased from Sigma Aldrich. All other chemicals employed were of analytical grade and used without further purification.

2.2 Synthesis of Bi–$Bi_2O_2CO_3$ Heterojunction

In a typical synthesis of Bi–$Bi_2O_2CO_3$, 0.2 millimol $Bi(NO_3)_3 \cdot 5H_2O$ was first dissolved in 20 mL 1 M HNO_3 (denoted as solution A). Meanwhile, 1.6 millimol Na_2CO_3 and 50 mg CTAB were dissolved in 20 mL ethanol–water mixture (denoted as solution B). Then, solution B was added into solution A under stirring for 30 min at 30 °C. The resulting mixture was transferred into a 20 mL Teflon-lined stainless-steel autoclave and was placed into an oven to react at 180 °C for 6 h. The system was then cooled to

ambient temperature naturally. The final product was collected and washed with distilled water and absolute alcohol at least five times. As-prepared samples were dried at 60 °C for 6 h. The reductive nature of EtOH and CTAB allowed an in situ formation of Bi nanoparticles on the $Bi_2O_2CO_3$ nanosheet. As a result, a heterojunction structure consisting of $Bi_2O_2CO_3$ sheets and metallic Bi nanoparticles has been produced. For the synthesis of $Bi_2O_2CO_3$ nanosheets we follow a preparation as reported by Zhou et al. [27].

2.3 Characterization Methods

Field emission scanning electron microscopy (FESEM, QUANTA FEG 250) was used to investigate the surface morphology of the samples and samples were performed by applying a diluted drop of samples on a silicon wafer. Transmission electron microscopy (TEM) grids were prepared by applying a diluted drop of the samples to carbon-coated copper grids. The particle sizes were determined from micrographs recorded at a magnification of 100,000X using an FEI (Technai S-Twin, operating at 200 kV) instrument. X-ray diffraction (XRD) patterns of the samples were recorded by employing a scanning rate of $0.02° S^{-1}$ in the 2θ range from 20° to 80° using a PANalytical XPERTPRO diffractometer equipped with Cu K_α radiation (at 40 mA and 40 kV). For optical experiments, the steady-state absorption and emission were carried out with a Shimadzu UV-2600 spectrophotometer and a Jobin–Yvon Fluoromax-3 fluorimeter, respectively. Picosecond-resolved spectroscopic studies were carried out using a commercial time correlated single photon counting (TCSPC) setup from Edinburgh Instruments (instrument response function, IRF = 80 ps, excitation at 375 nm). The details of experimental setting up and methodology were described in our earlier reports [41, 42].

2.4 Photocatalytic Performance Measurements

The photocatalysis activity of the samples were evaluated in terms of photodegradation of MB which was taken as a model pollutant in water. The photodegradation reaction of MB (initial concentration $C_0 = 0.5 \times 10^{-5}$ M) was carried out in a 10 mm optical path quartz cell reactor containing 2 mL of a model MB solution with a concentration of 0.5 g L^{-1} of the photocatalyst in deionized water (DI). The suspension was irradiated with a mercury lamp, $\lambda \geq 400$ nm (under visible light) and absorbance data were collected continuously by using a reported setting [4]. The percentage degradation (%DE) of MB was determined by Eq. 1:

$$\% \text{ DE } = \frac{I_0 - I}{I_0} \times 100 \tag{1}$$

where I_0 is the initial absorption intensity of MB at $\lambda_{max} = 660$ nm and I is the absorption intensity after irradiation.

2.5 Photocurrent Measurements

Photocurrent measurements were done in a dye-sensitized solar cell (DSSC) setup [43]. To prepare the working and counter electrodes for the photocurrent responses, FTO glasses were ultrasonically cleaned in soap-suds, deionized water, and acetone, respectively. For preparation of the counter electrode, platinum (Pt) was deposited on the FTO substrates by thermal decomposition of 10 mM platinum chloride (in isopropanol) at 385 °C for 30 min. $Bi_2O_2CO_3$ and $Bi–Bi_2O_2CO_3$ were used as the photoelectrode. The two electrodes were placed on top of each other with a single layer of 60 μm thick Surlyn (Solaronix) as a spacer between the two electrodes. A liquid electrolyte composed of 0.5 M lithium iodide (LiI), 0.05 M iodine (I_2) and 0.5 M 4-*tert*-butylpyridine (TBP) in acetonitrile was used as the hole conductor and filled in the inter electrode space using capillary force through two small holes (diameter = 1 mm) predrilled on the counter electrode. Finally, the two holes were sealed by using another piece of Surlyn to prevent a leakage of the electrolyte from the cell. In all our experiments, the active area of the DSSCs was fixed to 1 cm^2.

3 Results and Discussion

Figure 1a shows XRD patterns of the as-synthesized $Bi_2O_2CO_3$ and $Bi–Bi_2O_2CO_3$. The diffraction pattern of $Bi_2O_2CO_3$ is perfectly indicated as a tetragonal $Bi_2O_2CO_3$ phase. After the addition of ethanol, the XRD pattern of the $Bi–Bi_2O_2CO_3$ sample is also indexed to the $Bi_2O_2CO_3$ phase (JCPDS card no. 41-1488) [44]. No characteristic peak for Bi nanoparticles in $Bi–Bi_2O_2CO_3$ was observed, probably due to low content of Bi. Similar results were reported in previously literatures based on metal/semiconductor photocatalyst [35, 45, 46]. As shown in Fig. 1b, c, the SEM images of $Bi_2O_2CO_3$ and $Bi-Bi_2O_2CO_3$ reveal a large sheet-like morphology with a width from 50 to 600 nm. After decoration of Bi on the $Bi_2O_2CO_3$ nanosheets, no significant structural and morphological change was observed. The smooth sheet-like morphology of $Bi–Bi_2O_2CO_3$ indicates a uniform distribution of Bi nanoparticles on the surface of $Bi_2O_2CO_3$. Morphology and crystallinity of $Bi_2O_2CO_3$ and $Bi–Bi_2O_2CO_3$ were further examined via TEM and HRTEM as shown in Fig. 2a–d.
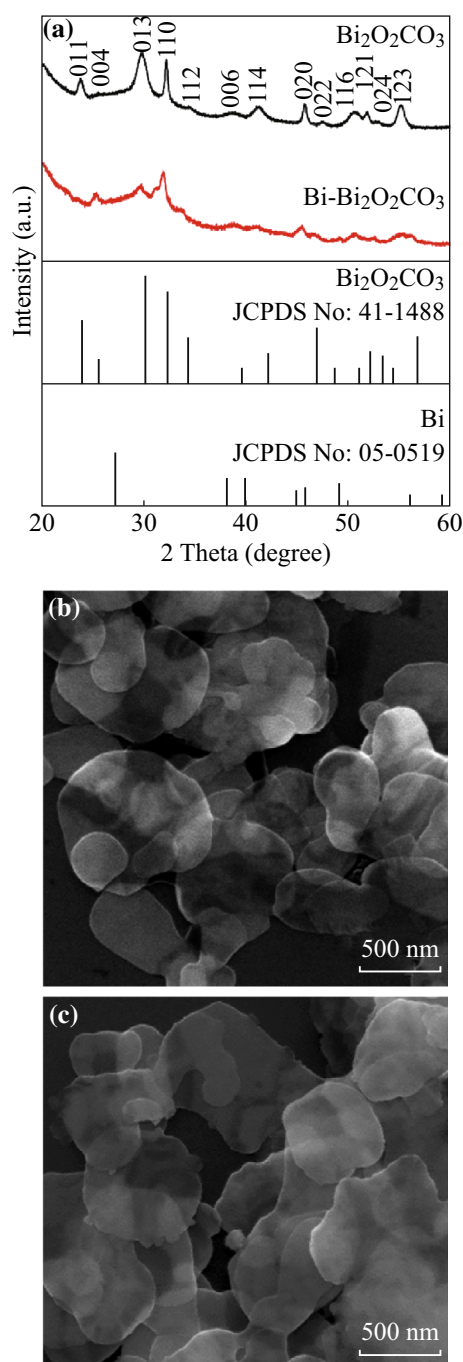
Fig. 1 **a** XRD patterns of $Bi_2O_2CO_3$ and $Bi–Bi_2O_2CO_3$. SEM images of **b** $Bi_2O_2CO_3$ and **c** $Bi–Bi_2O_2CO_3$

Fig. 2 TEM images of **a** $Bi_2O_2CO_3$ and **b** $Bi–Bi_2O_2CO_3$. HRTEM images of **c** $Bi_2O_2CO_3$ and **d** $Bi–Bi_2O_2CO_3$. SAED patterns of **e** $Bi_2O_2CO_3$ and **f** $Bi–Bi_2O_2CO_3$. **g** EDAX spectrum of $Bi_2O_2CO_3$ and $Bi–Bi_2O_2CO_3$

The TEM image of $Bi–Bi_2O_2CO_3$ shows a uniform distribution of Bi nanoparticles on the surface of the $Bi_2O_2CO_3$ nanosheets. The HRTEM images of $Bi_2O_2CO_3$ and $Bi–Bi_2O_2CO_3$ exhibit a high crystallinity of $Bi_2O_2CO_3$ nanosheet and Bi nanoparticles as given in Fig. 2c, d. The inter-planar distance between the fringes are about 0.276 and 0.32 nm, which correspond to the (110) crystal plane of $Bi_2O_2CO_3$ and (012) crystal plane of Bi nanoparticles,

respectively [38, 47]. The selected area electron diffraction (SAED) pattern obtained from the HRTEM images (Fig. 2e, f) demonstrates further the well-crystallinity. From the EDAX measurement shown in Fig. 2g, the at.% ratio of Bi and O is 1:5 for $Bi_2O_2CO_3$ whereas 2:3 for $Bi–Bi_2O_2CO_3$. The XPS studies of $Bi_2O_2CO_3$ and $Bi–Bi_2O_2CO_3$ were well documented in earlier studies [18, 27, 31, 48]. In those studies, they concluded that the O
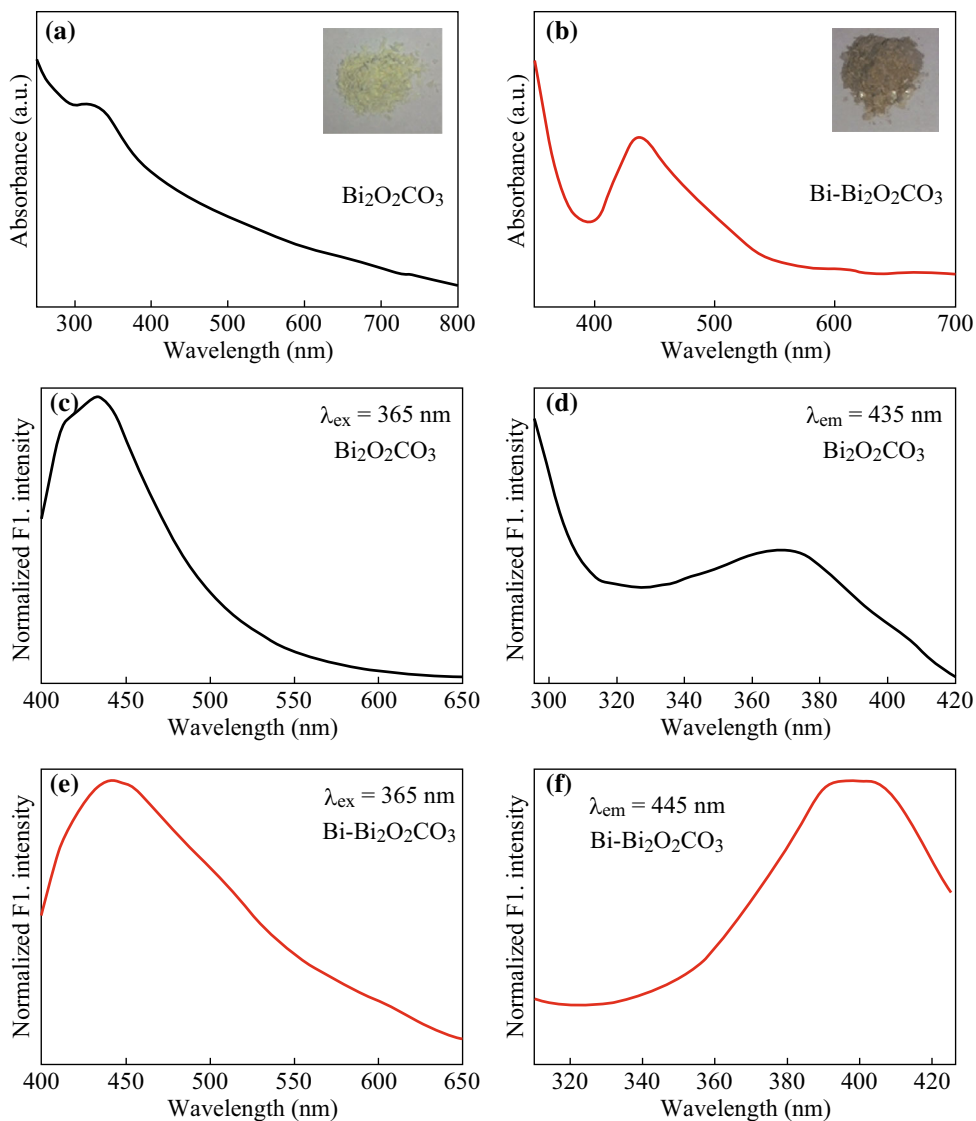
Fig. 3 UV-Vis absorption spectrum of **a** Bi$_2$O$_2$CO$_3$ and **b** Bi–Bi$_2$O$_2$CO$_3$ (*Inset* shows the image of Bi$_2$O$_2$CO$_3$ and Bi–Bi$_2$O$_2$CO$_3$). Normalized steady-steady PL spectrum of **c** Bi$_2$O$_2$CO$_3$ and **e** Bi–Bi$_2$O$_2$CO$_3$. The excitation spectrum of Bi$_2$O$_2$CO$_3$ **d** and Bi–Bi$_2$O$_2$CO$_3$ **f** at different PL maxima

1s peak centered at 530.5 eV ascribed to Bi–O bonds in Bi$_2$O$_2$CO$_3$, while peaks at 284.8 and 288.7 eV were the characteristic peaks of adventitious carbon species and CO$_3^{2-}$ in Bi$_2$O$_2$CO$_3$. Peaks around 157.0 and 162.3 eV were assigned to the formation of Bi metal present in the heterostructure. The other characterizations on Bi$_2$O$_2$CO$_3$ and Bi–Bi$_2$O$_2$CO$_3$ related materials [18, 27, 31, 48] including HRTEM and EDAX are consistent with our experimental observations.

Figure 3a shows UV–Vis absorption spectra of Bi$_2$O$_2$CO$_3$ and Bi–Bi$_2$O$_2$CO$_3$. The Bi$_2$O$_2$CO$_3$ shows absorption peak at 360 nm and long tail over 800 nm due to scattering of the nanoparticles presented in the solution, which consists with earlier reports [49, 50]. After formation of
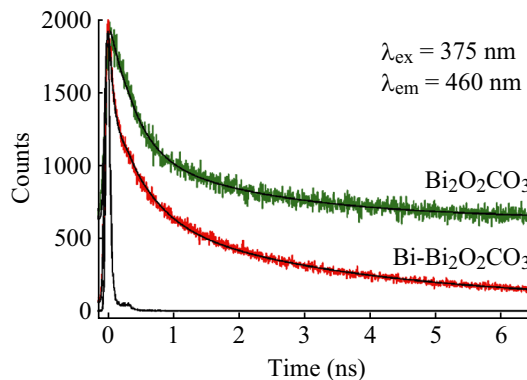

Fig. 4 Picosecond-resolved PL transients of Bi$_2$O$_2$CO$_3$ and Bi–Bi$_2$O$_2$CO$_3$ measured at $\lambda_{em} = 460$ nm upon $\lambda_{ex} = 375$ nm

Table 1 Lifetimes of picosecond time-resolved PL transients of $Bi_2O_2CO_3$ and $Bi-Bi_2O_2CO_3$ detected at 460 nm PL maxima uopn excitation at 375 nm wavelength

System	τ_1 (ps)	τ_2 (ps)	τ_3 (ps)	τ_{avg} (ns)
$Bi_2O_2CO_3$	343 (71%)	3500 (29%)		1.25
$Bi-Bi_2O_2CO_3$	50 (58%)	394 (25%)	3400 (17%)	0.70

The values in parentheses represent the relative weight percentages of the time components

heterojunction $Bi-Bi_2O_2CO_3$, an enhancement of absorption in the visible region was observed due to the presence of Bi nanoparticles, and surface plasmon absorption around 500 nm was found as shown in Fig. 3b. The SPR of non-noble metal Bi in the near ultraviolet and visible region were reported by different groups [51, 52]. Notably, such absorption enhancement in the visible region is also according to the color change of the samples as shown in the inset of Fig. 3a, b. Thus, formation of Bi nanoparticles on the surface of $Bi_2O_2CO_3$ nanosheets results in an enhancement of absorption over the entire UV–Vis region. The photoluminescences of $Bi_2O_2CO_3$ and $Bi-Bi_2O_2CO_3$ exhibit emission around 400–550 nm upon excitation at 365 nm as shown in Fig. 3c, e. Picosecond-resolved fluorescence was studied to investigate the detailed photophysical properties of the heterostructure after decoration of Bi nanoparticles on the $Bi_2O_2CO_3$ nanosheets. The fluorescence decay of $Bi_2O_2CO_3$ and $Bi-Bi_2O_2CO_3$ was determined at 460 nm upon excitation by 375 nm laser source (Fig. 4) and tabulated in Table 1.

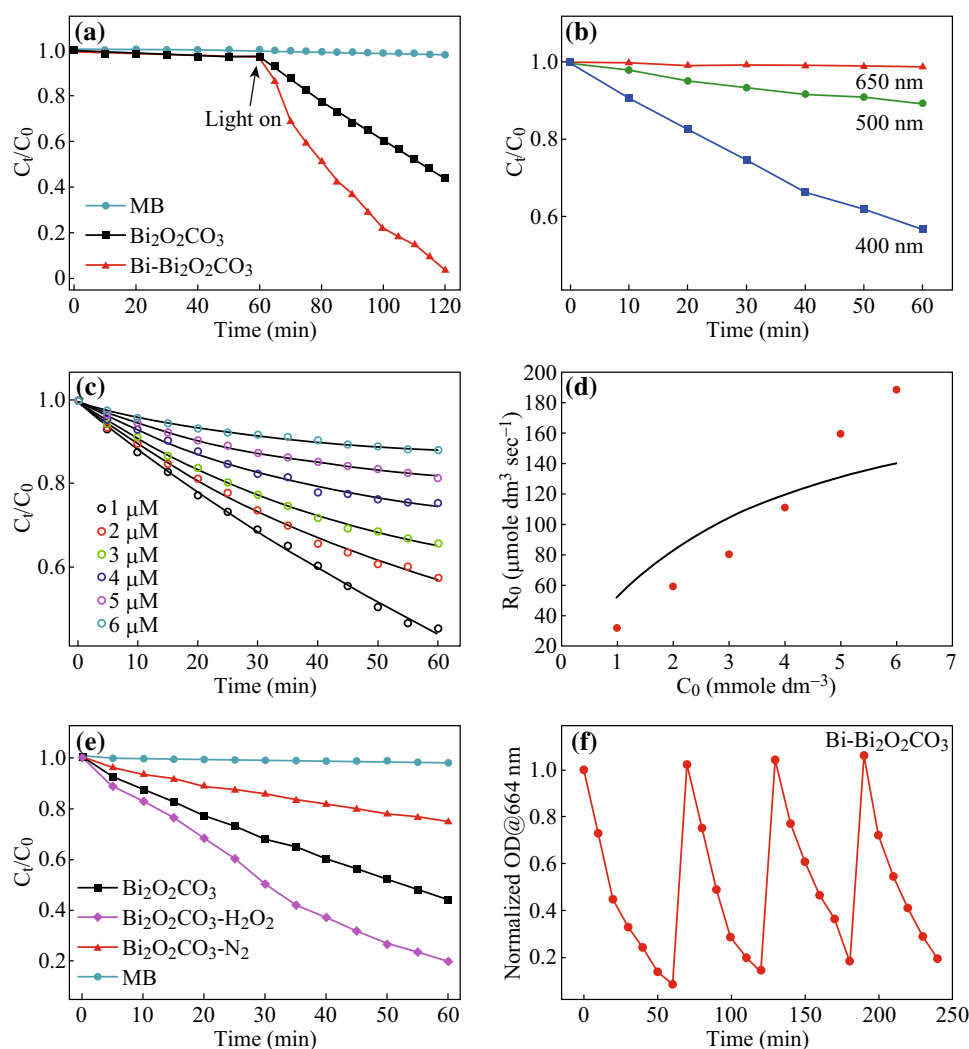**Fig. 5 a** Photocatalytic degradation of MB under visible light illumination. **b** Photocatalytic degradation of MB by $Bi_2O_2CO_3$ at different wavelength. **c** C_t/C_0 versus time with various concentrations of methylene blue by $Bi_2O_2CO_3$. **d** Langmuir–Hinshelwood plot (L–H) for photocatalytic degradation of methylene blue using $Bi_2O_2CO_3$ (*solid line* is the model fitting and *solid circles* are experimental data). **e** Photodegradation of MB over $Bi_2O_2CO_3$ and $Bi–Bi_2O_2CO_3$ under conventional condition, presence of H_2O_2 and N_2 into the solution. **f** A recyclability study of $Bi–Bi_2O_2CO_3$ under visible light illumination

The fluorescence decay of $Bi_2O_2CO_3$ shows two components of 343 ps and 3.5 ns along with an average lifetime of 1.25 ns. After decoration of Bi nanoparticles, the average time of $Bi-Bi_2O_2CO_3$ decreases to 0.70 ns. Thus, the faster component of 50 ps is attributed to the excited state electron transfer from $Bi_2O_2CO_3$ to Bi. The obvious decrease in fluorescence lifetime of the heterostructures suggests that the decoration of Bi nanoparticles on the $Bi_2O_2CO_3$ nanosheets can act as electron sink and therefore contribute to electron–hole separation. Such kind of metal-semiconductor heterojunctions facilitates in a remarkable way of the decline in the recombination of electron–hole pairs and is useful to enhance solar energy utilization [53–55].

The photocatalytic activities of $Bi_2O_2CO_3$ and $Bi-Bi_2O_2CO_3$ were evaluated by photodegradation of the model organic contaminant MB under visible light illumination. However, in our case the as-prepared $Bi_2O_2CO_3$ and $Bi-Bi_2O_2CO_3$ have insignificant photocatalytic activity in dark (Fig. 5a). During the photocatalytic reaction, MB forms a well-known colorless product leucomethylene blue (LMB) [56, 57] as expressed in Eq. 2.

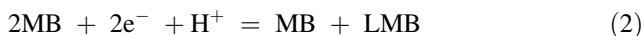$$2MB + 2e^- + H^+ = MB + LMB \qquad (2)$$

Figure 5a shows changes in MB concentration as a function of time in presence and absence of photocatalysts. With our experimental time window, MB has less than 10% degradation under light illumination in the absence of photocatalysts. In contrast, $Bi_2O_2CO_3$ nanosheets show an enhanced photocatalytic activity and 60% of MB was degraded after 60 min illumination. One can see that presence of Bi nanoparticles on the $Bi_2O_2CO_3$ nanosheets further enhance photocatalytic activity (100%) compared to $Bi_2O_2CO_3$ nanosheets (60%). Figure 5b shows photocatalysis of methylene blue (MB) at different wavelength by $Bi_2O_2CO_3$. Insignificant photocatalysis at 650 nm (MB absorbance maxima 660 nm) indicates that MB is unable to photosensitize $Bi_2O_2CO_3$. Thus photocatalysis predominately takes place via sensitization of $Bi_2O_2CO_3$. In order to find out the effect of the surface on photocatalysis, the Langmuir–Hinshelwood (L–H) kinetics was studied using different concentrations of MB (Fig. 5c). As shown in Fig. 5d, a significant deviation of the model (solid line) from experimental data is evident. The observation indicates that surface adsorption of the model pollutant plays insignificant role in the photodegradation. In order to investigate the catalytic pathway, we further studied the photocatalytic activity of $Bi_2O_2CO_3$ in the presence of a radical initiator (H_2O_2) and radical quencher (N_2 bubbling) separately (Fig. 5e). In fact, in the presence of H_2O_2 under solar light illumination increases generation of OH· which eventually increases the photocatalytic activity of $Bi_2O_2CO_3$ for degradation of MB. This demonstrates the role of

reactive oxygen species (ROS) in the degradation of MB [58]. The photodegradation efficiency of $Bi_2O_2CO_3$ decreases with N_2 bubbling in the solution, so O_2 primarily acts as an efficient electron trap, leading to the generation of O_2^- radicals during photocatalytic reaction [59]. From the application point of view, photochemical stability and durability of photocatalysts are significant during photocatalytic reaction [60]. To further test photocatalytic performance of the as-prepared heterojunction $Bi-Bi_2O_2CO_3$ photocatalyst, recycling experiment was carried out under repeated irradiation. Figure 5f shows the repeated photocatalytic activity of $Bi-Bi_2O_2CO_3$. The results indicate that the rate remains similar after four consecutive cycles, implying that the obtained $Bi-Bi_2O_2CO_3$ heterojunction photocatalyst has high stability and no photocorrosion occurs during the photodegradation of MB. Photocurrent measurement was carried out under solar light illumination to investigate the efficient electron–hole separation. The photocurrent of $Bi-Bi_2O_2CO_3$ heterostructures is much higher than that of $Bi_2O_2CO_3$ (see Fig. 6). This implies that the heterojunction shows an improved separation of photogenerated electron–hole pairs and can greatly facilitate its photocatalytic activity.

There are several reports which indicate that the enhancement in photocatalytic performance can be ascribed to the synergetic effects of many factors, such as hierarchical structure, surface area, interfacial charge transfer, and efficient separation of photoinduced electrons and holes [61–65]. In the present study, the enhanced photocatalytic performance for the $Bi-Bi_2O_2CO_3$ photocatalyst can be ascribed to the formation of heterojunction between Bi nanoparticles and the surface of $Bi_2O_2CO_3$ nanosheets. Furthermore, the Fermi level of Bi nanoparticles which acts as electron acceptors can be estimated to be about -0.17 eV as calculated by the work function of metallic bismuth of 4.22 eV [66–68]. Since the Fermi level of metallic Bi (-0.17 eV) is lower than the conduction band of $Bi_2O_2CO_3$ (-1.40 eV) [27], the photogenerated
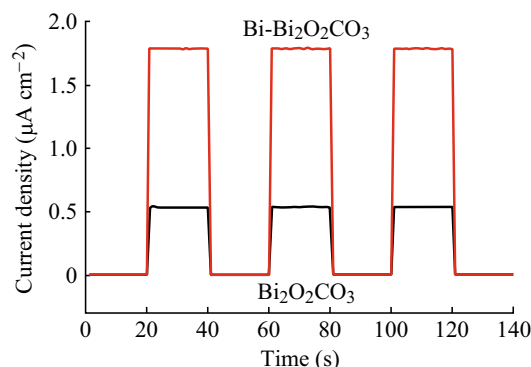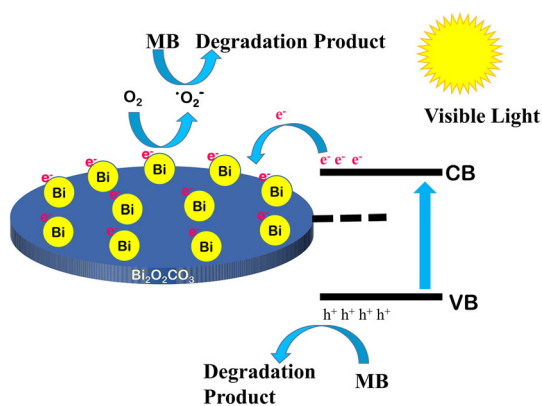

Fig. 6 Current–time curves of electrodes made of pure $Bi_2O_2CO_3$ and $Bi–Bi_2O_2CO_3$ heterojunction

Scheme 1 Schematic illustration of enhanced photocatalytic activity by Bi–$Bi_2O_2CO_3$ heterojunction under visible light illumination

electrons would probably transfer from $Bi_2O_2CO_3$ to the deposited Bi nanoparticles and therefore promote the separation of photo-generated electrons and holes, effectively. After the separation of electrons and holes, these two kinds of photogenerated charge carriers would be transformed into reactive species that are responsible for promoting photocatalytic activity. Based on the above investigations, a schematic illustration is proposed as shown in Scheme 1.

4 Conclusion

We successfully synthesized Bi–$Bi_2O_2CO_3$ heterojunction by a one-step hydrothermal method. Detailed spectroscopic investigations reveal that ultrafast photo-induced charge separation in the Bi–$Bi_2O_2CO_3$ heterojunction is conducive for enhanced solar energy conversion. As a potential prototype application, we found enhanced photocatalytic activity of the heterostructure using MB as a model organic contaminant under visible light illumination. The efficient separation of photoinduced electron–hole pairs in the heterojunction was further proved by photocurrent measurement. Moreover, this work not only provides cost effective procedure to prepare efficient photocatalyst with high stability but also opens up a new field for bismuth containing heterostructures with several future applications.

References

1. M.N. Chong, B. Jin, C.W.K. Chow, C. Saint, Recent developments in photocatalytic water treatment technology: a review. Water Res. **44**(10), 2997–3027 (2010). doi:10.1016/j.watres.2010.02.039
2. M.R. Hoffmann, S.T. Martin, W. Choi, D.W. Bahnemann, Environmental applications of semiconductor photocatalysis. Chem. Rev. **95**(1), 69–96 (1995). doi:10.1021/cr00033a004
3. S. Dong, J. Feng, M. Fan, Y. Pi, L. Hu, X. Han, M. Liu, J. Sun, Recent developments in heterogeneous photocatalytic water treatment using visible light-responsive photocatalysts: a review. RSC Adv. **5**(19), 14610–14630 (2015). doi:10.1039/C4RA13734E
4. Sunil P. Lonkar, Vishnu V. Pillai, Samuel Stephen, Ahmed Abdala, Vikas Mittal, Facile in situ fabrication of nanostructured graphene-CuO hybrid with hydrogen sulfide removal capacity. Nano-Micro Lett. **8**(4), 312–319 (2016). doi:10.1007/s40820-016-0090-8
5. P. Kar, S. Sardar, S. Ghosh, M.R. Parida, B. Liu, O.F. Mohammed, P. Lemmens, S.K. Pal, Nano surface engineering of Mn_2O_3 for potential light-harvesting application. J. Mater. Chem. C **3**(31), 8200–8211 (2015). doi:10.1039/C5TC01475A
6. T.K. Maji, D. Bagchi, P. Kar, D. Karmakar, S.K. Pal, Enhanced charge separation through modulation of defect-state in wide band-gap semiconductor for potential photocatalysis application: Ultrafast spectroscopy and computational studies. J. Photochem. Photobiol. A **332**, 391–398 (2017). doi:10.1016/j.jphotochem.2016.09.017
7. Y. Wang, Q. Wang, X. Zhan, F. Wang, M. Safdar, J. He, Visible light driven type II heterostructures and their enhanced photocatalysis properties: a review. Nanoscale **5**(18), 8326–8339 (2013). doi:10.1039/c3nr01577g
8. J. Liqiang, S. Xiaojun, S. Jing, C. Weimin, X. Zili, D. Yaoguo, F. Honggang, Review of surface photovoltage spectra of nano-sized semiconductor and its applications in heterogeneous photocatalysis. Sol. Energy Mater. Sol. Cells **79**(2), 133–151 (2003). doi:10.1016/S0927-0248(02)00393-8
9. H. Huang, X. Li, J. Wang, F. Dong, P.K. Chu, T. Zhang, Y. Zhang, Anionic group self-doping as a promising strategy: band-gap engineering and multi-functional applications of high-performance CO_{32}-doped $Bi_2O_2CO_3$. ACS Catal. **5**(7), 4094–4103 (2015). doi:10.1021/acscatal.5b00444
10. H. Huang, X. Han, X. Li, S. Wang, P.K. Chu, Y. Zhang, Fabrication of multiple heterojunctions with tunable visible-light-active photocatalytic reactivity in BiOBr–BiOI full-range composites based on microstructure modulation and band structures. ACS Appl. Mater. Interfaces **7**(1), 482–492 (2015). doi:10.1021/am5065409
11. H. Huang, K. Xiao, Y. He, T. Zhang, F. Dong, X. Du, Y. Zhang, In situ assembly of BiOI@$Bi_{12}O_{17}Cl_2$ p-n junction: charge induced unique front-lateral surfaces coupling heterostructure with high exposure of BiOI {001} active facets for robust and nonselective photocatalysis. Appl. Catal. B **199**, 75–86 (2016). doi:10.1016/j.apcatb.2016.06.020

12. H. Huang, K. Liu, K. Chen, Y. Zhang, Y. Zhang, S. Wang, Ce and F comodification on the crystal structure and enhanced photocatalytic activity of Bi_2WO_6 photocatalyst under visible light irradiation. J. Phys. Chem. C 118(26), 14379–14387 (2014). doi:10.1021/jp503025b

13. Q. He, S. Huang, C. Wang, Q. Qiao, N. Liang, M. Xu, W. Chen, J. Zai, X. Qian, The role of Mott-Schottky heterojunctions in Ag–Ag8SnS6 as counter electrodes in dye-sensitized solar cells. Chem. Sus. Chem. 8(5), 817–820 (2015). doi:10.1002/cssc.201403343

14. S. Huang, Q. He, J. Zai, M. Wang, X. Li, B. Li, X. Qian, The role of Mott-Schottky heterojunctions in PtCo-Cu_2ZnGeS_4 as counter electrodes in dye-sensitized solar cells. Chem. Commun. 51(43), 8950–8953 (2015). doi:10.1039/C5CC02584B

15. L. Jin, G. Zhu, M. Hojamberdiev, X. Luo, C. Tan, J. Peng, X. Wei, J. Li, P. Liu, A plasmonic Ag–$AgBr/Bi_2O_2CO_3$ composite photocatalyst with enhanced visible-light photocatalytic activity. Ind. Eng. Chem. Res. 53(35), 13718–13727 (2014). doi:10.1021/ie502133x

16. G. Zhu, M. Hojamberdiev, K.-I. Katsumata, X. Cai, N. Matsushita, K. Okada, P. Liu, J. Zhou, Heterostructured $Fe_3O_4/Bi_2O_2CO_3$ photocatalyst: synthesis, characterization and application in recyclable photodegradation of organic dyes under visible light irradiation. Mater. Chem. Phys. 142(1), 95–105 (2013). doi:10.1016/j.matchemphys.2013.06.046

17. A. Hameed, T. Montini, V. Gombac, P. Fornasiero, Surface phases and photocatalytic activity correlation of Bi_2O_3/Bi_2O_{4-x} nanocomposite. J. Am. Chem. Soc. 130(30), 9658–9659 (2008). doi:10.1021/ja803603y

18. S. Xiao, Y. Li, J. Hu, H. Li, X. Zhang, L. Liu, J. Lian, One-step synthesis of nanostructured Bi-$Bi_2O_2CO_3$-ZnO composites with enhanced photocatalytic performance. Cryst. Eng. Comm. 17(20), 3809–3819 (2015). doi:10.1039/C5CE00338E

19. P. Cai, S. Zhou, D. Ma, S. Liu, W. Chen, S. Huang, Fe_2O_3-modified porous $BiVO_4$ nanoplates with enhanced photocatalytic activity. Nano-Micro Lett. 7(2), 183–193 (2015). doi:10.1007/s40820-015-0033-9

20. W. Wang, J. Wang, Z. Wang, X. Wei, L. Liu, Q. Ren, W. Gao, Y. Liang, H. Shi, p-n junction $CuO/BiVO_4$ heterogeneous nanostructures: synthesis and highly efficient visible-light photocatalytic performance. Dalton Trans. 43(18), 6735–6743 (2014). doi:10.1039/c3dt53613k

21. Y. Zhang, G. Zhu, M. Hojamberdiev, J. Gao, J. Hao, J. Zhou, P. Liu, Synergistic effect of oxygen vacancy and nitrogen doping on enhancing the photocatalytic activity of $Bi_2O_2CO_3$ nanosheets with exposed {001} facets for the degradation of organic pollutants. Appl. Surf. Sci. 371, 231–241 (2016). doi:10.1016/j.apsusc.2016.02.210

22. C. Greaves, S.K. Blower, Structural relationships between $Bi_2O_2CO_3$ and β-Bi_2O_3. Mater. Res. Bull. 23(7), 1001–1008 (1988). doi:10.1016/0025-5408(88)90055-4

23. P. Madhusudan, J. Zhang, B. Cheng, G. Liu, Photocatalytic degradation of organic dyes with hierarchical $Bi_2O_2CO_3$ microstructures under visible-light. CrystEngComm 15(2), 231–240 (2013). doi:10.1039/C2CE26639C

24. T. Zhao, J. Zai, M. Xu, Q. Zou, Y. Su, K. Wang, X. Qian, Hierarchical $Bi_2O_2CO_3$ microspheres with improved visible-light-driven photocatalytic activity. CrystEngComm 13(12), 4010–4017 (2011). doi:10.1039/c1ce05113j

25. P. Madhusudan, J. Yu, W. Wang, B. Cheng, G. Liu, Facile synthesis of novel hierarchical graphene-$Bi_2O_2CO_3$ composites with enhanced photocatalytic performance under visible light. Dalton Trans. 41(47), 14345–14353 (2012). doi:10.1039/c2dt31528a

26. Y.-S. Xu, W.-D. Zhang, Anion exchange strategy for construction of sesame-biscuit-like $Bi_2O_2CO_3/Bi_2MoO_6$ nanocomposites with enhanced photocatalytic activity. Appl. Catal. B 140–141, 306–316 (2013). doi:10.1016/j.apcatb.2013.04.019

27. Z. Zhao, Y. Zhou, F. Wang, K. Zhang, S. Yu, K. Cao, Polyaniline-decorated {001} facets of $Bi_2O_2CO_3$ nanosheets: in situ oxygen vacancy formation and enhanced visible light photocatalytic activity. ACS Appl. Mater. Interfaces 7(1), 730–737 (2015). doi:10.1021/am507089x

28. N. Liang, M. Wang, L. Jin, S. Huang, W. Chen et al., Highly efficient $Ag_2O/Bi_2O_2CO_3$ p-n heterojunction photocatalysts with improved visible-light responsive activity. ACS Appl. Mater. Interfaces 6(14), 11698–11705 (2014). doi:10.1021/am502481z

29. S. Peng, L. Li, H. Tan, Y. Wu, R. Cai et al., Monodispersed Ag nanoparticles loaded on the PVP-assisted synthetic $Bi_2O_2CO_3$ microspheres with enhanced photocatalytic and supercapacitive performances. J. Mater. Chem. A 1(26), 7630–7638 (2013). doi:10.1039/c3ta10951h

30. R. Wang, X. Li, W. Cui, Y. Zhang, F. Dong, In situ growth of Au nanoparticles on 3D $Bi_2O_2CO_3$ for surface plasmon enhanced visible light photocatalysis. New J. Chem. 39(11), 8446–8453 (2015). doi:10.1039/C5NJ01882J

31. F. Dong, Q. Li, Y. Sun, W.-K. Ho, Noble metal-like behavior of plasmonic Bi particles as a cocatalyst deposited on $(BiO)_2CO_3$ microspheres for efficient visible light photocatalysis. ACS Catal. 4(12), 4341–4350 (2014). doi:10.1021/cs501038q

32. H. Safardoust-Hojaghan, M. Salavati-Niasari, M.H. Motaghedifard, S.M. Hosseinpour-Mashkani, Synthesis of micro sphere-like bismuth nanoparticles by microwave assisted polyol method; designing a novel electrochemical nanosensor for ultra-trace measurement of Pb^{2+} ions. New J. Chem. 39(6), 4676–4684 (2015). doi:10.1039/C5NJ00532A

33. Z. Wang, C. Jiang, R. Huang, H. Peng, X. Tang, Investigation of optical and photocatalytic properties of bismuth nanospheres prepared by a facile thermolysis method. J. Phys. Chem. C 118(2), 1155–1160 (2014). doi:10.1021/jp4065505

34. F. Dong, T. Xiong, Y. Sun, Z. Zhao, Y. Zhou, X. Feng, Z. Wu, A semimetal bismuth element as a direct plasmonic photocatalyst. Chem. Commun. 50(72), 10386–10389 (2014). doi:10.1039/C4CC02724H

35. D. Chen, M. Zhang, Q. Lu, J. Chen, B. Liu, Z. Wang, Facile synthesis of Bi/BiOCl composite with selective photocatalytic properties. J. Alloys Compd. 646, 647–654 (2015). doi:10.1016/j.jallcom.2015.06.113

36. Y. Huang, W. Wang, Q. Zhang, J.-J. Cao, R.-J. Huang, W. Ho, S.C. Lee, In situ fabrication of α-$Bi_2O_3/(BiO)_2CO_3$ nanoplate heterojunctions with tunable optical property and photocatalytic activity. Sci. Rep. 6, 23435 (2016). doi:10.1038/srep23435

37. C. Chang, L. Zhu, Y. Fu, X. Chu, Highly active Bi/BiOI composite synthesized by one-step reaction and its capacity to degrade bisphenol A under simulated solar light irradiation. Chem. Eng. J. 233, 305–314 (2013). doi:10.1016/j.cej.2013.08.048

38. M. Gao, D. Zhang, X. Pu, H. Li, D. Lv, B. Zhang, X. Shao, Facile hydrothermal synthesis of Bi/BiOBr composites with enhanced visible-light photocatalytic activities for the degradation of rhodamine B. Sep. Purif. Technol. 154, 211–216 (2015). doi:10.1016/j.seppur.2015.09.063

39. Y. Chen, D. Chen, J. Chen, Q. Lu, M. Zhang, B. Liu, Q. Wang, Z. Wang, Facile synthesis of Bi nanoparticle modified TiO_2 with enhanced visible light photocatalytic activity. J. Alloys Compd. 651, 114–120 (2015). doi:10.1016/j.jallcom.2015.08.119

40. X. Liu, H. Cao, J. Yin, Generation and photocatalytic activities of $Bi@Bi_2O_3$ microspheres. Nano Res. 4(5), 470–482 (2011). doi:10.1007/s12274-011-0103-3

41. S. Sardar, P. Kar, S. Sarkar, P. Lemmens, S.K. Pal, Interfacial carrier dynamics in PbS-ZnO light harvesting assemblies and their potential implication in photovoltaic/photocatalysis application. Sol. Energ. Mat. Sol. Cells 134, 400–406 (2015). doi:10.1016/j.solmat.2014.12.032

42. P.K. Sarkar, N. Polley, S. Chakrabarti, P. Lemmens, S.K. Pal, Nanosurface energy transfer based highly selective and ultra-sensitive "Turn on" fluorescence mercury sensor. ACS Sens. **1**(6), 789–797 (2016). doi:10.1021/acssensors.6b00153

43. S. Sardar, P. Kar, H. Remita, B. Liu, P. Lemmens, S. Kumar Pal, S. Ghosh, Enhanced charge separation and FRET at heterojunctions between semiconductor nanoparticles and conducting polymer nanofibers for efficient solar light harvesting. Sci. Rep. **5**, 17313 (2015). doi:10.1038/srep17313

44. Y. Sun, Z. Zhao, F. Dong, W. Zhang, Mechanism of visible light photocatalytic NO_x oxidation with plasmonic Bi cocatalyst-enhanced $(BiO)_2CO_3$ hierarchical microspheres. Phys. Chem. Chem. Phys. **17**(16), 10383–10390 (2015). doi:10.1039/C4CP06045H

45. J.L.T. Chen, V. Nalla, G. Kannaiyan, V. Mamidala, W. Ji, J.J. Vittal, Synthesis and nonlinear optical switching of Bi_2S_3 nanorods and enhancement in the NLO response of Bi_2S_3@Au nanorod-composites. New J. Chem. **38**(3), 985–992 (2014). doi:10.1039/c3nj01380d

46. S.P. Lim, A. Pandikumar, N.M. Huang, H.N. Lim, Facile synthesis of Au@TiO_2 nanocomposite and its application as a photoanode in dye-sensitized solar cells. RSC Adv. **5**(55), 44398–44407 (2015). doi:10.1039/C5RA06220A

47. G. Cheng, H. Yang, K. Rong, Z. Lu, X. Yu, R. Chen, Shape-controlled solvothermal synthesis of bismuth subcarbonate nanomaterials. J. Solid State Chem. **183**(8), 1878–1883 (2010). doi:10.1016/j.jssc.2010.06.004

48. G. Zhu, Y. Liu, M. Hojamberdiev, J. Han, J. Rodriguez, S.A. Bilmes, P. Liu, Thermodecomposition synthesis of porous β-Bi_2O_3/$Bi_2O_2CO_3$ heterostructured photocatalysts with improved visible light photocatalytic activity. New J. Chem. **39**(12), 9557–9568 (2015). doi:10.1039/C5NJ01462J

49. S. Lin, L. Liu, Y. Liang, W. Cui, Z. Zhang, Oil-in-water self-assembled synthesis of Ag@AgCl nano-particles on flower-like $Bi_2O_2CO_3$ with enhanced visible-light-driven photocatalytic activity. Materials **9**(6), 486 (2016). doi:10.3390/ma9060486

50. J. Siegel, O. Kvítek, P. Ulbrich, Z. Kolská, P. Slepička, V. Švorčík, Progressive approach for metal nanoparticle synthesis. Mater. Lett. **89**, 47–50 (2012). doi:10.1016/j.matlet.2012.08.048

51. S. Weng, B. Chen, L. Xie, Z. Zheng, P. Liu, Facile in situ synthesis of a Bi/BiOCl nanocomposite with high photocatalytic activity. J. Mater. Chem. A **1**(9), 3068–3075 (2013). doi:10.1039/c2ta01004f

52. J. Toudert, R. Serna, M. Jiménez de Castro, Exploring the optical potential of nano-bismuth: tunable surface plasmon resonances in the near ultraviolet-to-near infrared range. J. Phys. Chem. C **116**(38), 20530–20539 (2012). doi:10.1021/jp3065882

53. S.K. Cushing, N. Wu, Progress and perspectives of plasmon-enhanced solar energy conversion. J. Phys. Chem. Lett. **7**(4), 666–675 (2016). doi:10.1021/acs.jpclett.5b02393

54. J. Li, S.K. Cushing, F. Meng, T.R. Senty, A.D. Bristow, N. Wu, Plasmon-induced resonance energy transfer for solar energy conversion. Nat. Photon. **9**(9), 601–607 (2015). doi:10.1038/nphoton.2015.142

55. R. Costi, A.E. Saunders, E. Elmalem, A. Salant, U. Banin, Visible light-induced charge retention and photocatalysis with hybrid CdSe–Au nanodumbbells. Nano Lett. **8**(2), 637–641 (2008). doi:10.1021/nl0730514

56. C. Yogi, K. Kojima, N. Wada, H. Tokumoto, T. Takai, T. Mizoguchi, H. Tamiaki, Photocatalytic degradation of methylene blue by TiO_2 film and Au particles-TiO_2 composite film. Thin Solid Films **516**(17), 5881–5884 (2008). doi:10.1016/j.tsf.2007.10.050

57. A. Mills, J. Wang, Photobleaching of methylene blue sensitised by TiO_2: an ambiguous system? J. Photochem. Photobiol. A **127**(1–3), 123–134 (1999). doi:10.1016/S1010-6030(99)00143-4

58. A. Giri, N. Goswami, M. Pal, M.T. Zar Myint, S. Al-Harthi, A. Singha, B. Ghosh, J. Dutta, S.K. Pal, Rational surface modification of Mn_3O_4 nanoparticles to induce multiple photoluminescence and room temperature ferromagnetism. J. Mater. Chem. C **1**(9), 1885–1895 (2013). doi:10.1039/c3tc00709j

59. Y. Park, S.-H. Lee, S.O. Kang, W. Choi, Organic dye-sensitized TiO_2 for the redox conversion of water pollutants under visible light. Chem. Commun. **46**(14), 2477–2479 (2010). doi:10.1039/b924829c

60. Z. Ai, W. Ho, S. Lee, L. Zhang, Efficient photocatalytic removal of NO in indoor air with hierarchical bismuth oxybromide nanoplate microspheres under visible light. Environ. Sci. Technol. **43**(11), 4143–4150 (2009). doi:10.1021/es9004366

61. F. Dong, Y. Sun, M. Fu, Z. Wu, S.C. Lee, Room temperature synthesis and highly enhanced visible light photocatalytic activity of porous BiOI/BiOCl composites nanoplates microflowers. J. Hazard. Mater. **219–220**, 26–34 (2012). doi:10.1016/j.jhazmat.2012.03.015

62. Q. Xiang, J. Yu, M. Jaroniec, Graphene-based semiconductor photocatalysts. Chem. Soc. Rev. **41**(2), 782–796 (2012). doi:10.1039/C1CS15172J

63. Q. Li, H. Liu, F. Dong, M. Fu, Hydrothermal formation of N-doped $(BiO)_2CO_3$ honeycomb-like microspheres photocatalysts with bismuth citrate and dicyandiamide as precursors. J. Colloid Interface Sci. **408**, 33–42 (2013). doi:10.1016/j.jcis.2013.07.040

64. S. Yu, H. Huang, F. Dong, M. Li, N. Tian, T. Zhang, Y. Zhang, Synchronously achieving plasmonic Bi metal deposition and I^- doping by utilizing $BiOIO_3$ as the self-sacrificing template for high-performance multifunctional applications. ACS Appl. Mater. Interfaces **7**(50), 27925–27933 (2015). doi:10.1021/acsami.5b09994

65. Y. Guo, Y. Zhang, N. Tian, H. Huang, Homogeneous {001}-BiOBr/Bi heterojunctions: facile controllable synthesis and morphology-dependent photocatalytic activity. ACS Sustain. Chem. Eng. **4**(7), 4003–4012 (2016). doi:10.1021/acssuschemeng.6b00884

66. V. Subramanian, E.E. Wolf, P.V. Kamat, Catalysis with TiO_2/gold nanocomposites. Effect of metal particle size on the fermi level equilibration. J. Am. Chem. Soc. **126**(15), 4943–4950 (2004). doi:10.1021/ja0315199

67. S. Trasatti, Electronegativity, work function, and heat of adsorption of hydrogen on metals. J. Chem. Soc. Faraday Trans. 1 **68**, 229–236 (1972). doi:10.1039/f19726800229

68. Y. Yu, C. Cao, H. Liu, P. Li, F. Wei, Y. Jiang, W. Song, A Bi/BiOCl heterojunction photocatalyst with enhanced electron-hole separation and excellent visible light photodegrading activity. J. Mater. Chem. A **2**(6), 1677–1681 (2014). doi:10.1039/C3TA14494A